iScience, Volume *26*

Supplemental information

A tumor microenvironment-associated circRNA predictor for tumor relapse and chemotherapy vulnerability in nasopharyngeal carcinoma

Ye-Lin Liang, Yu-Heng Zhao, Cong Ding, Sai-Wei Huang, Qian Li, Chong-Mei Zhu, Qing-Mei He, Ling-Long Tang, Yan-Ping Mao, Lei Chen, Wen-Fei Li, Guan-Qun Zhou, Na Liu, Wei Jiang, Jun Ma, and Ying-Qin Li

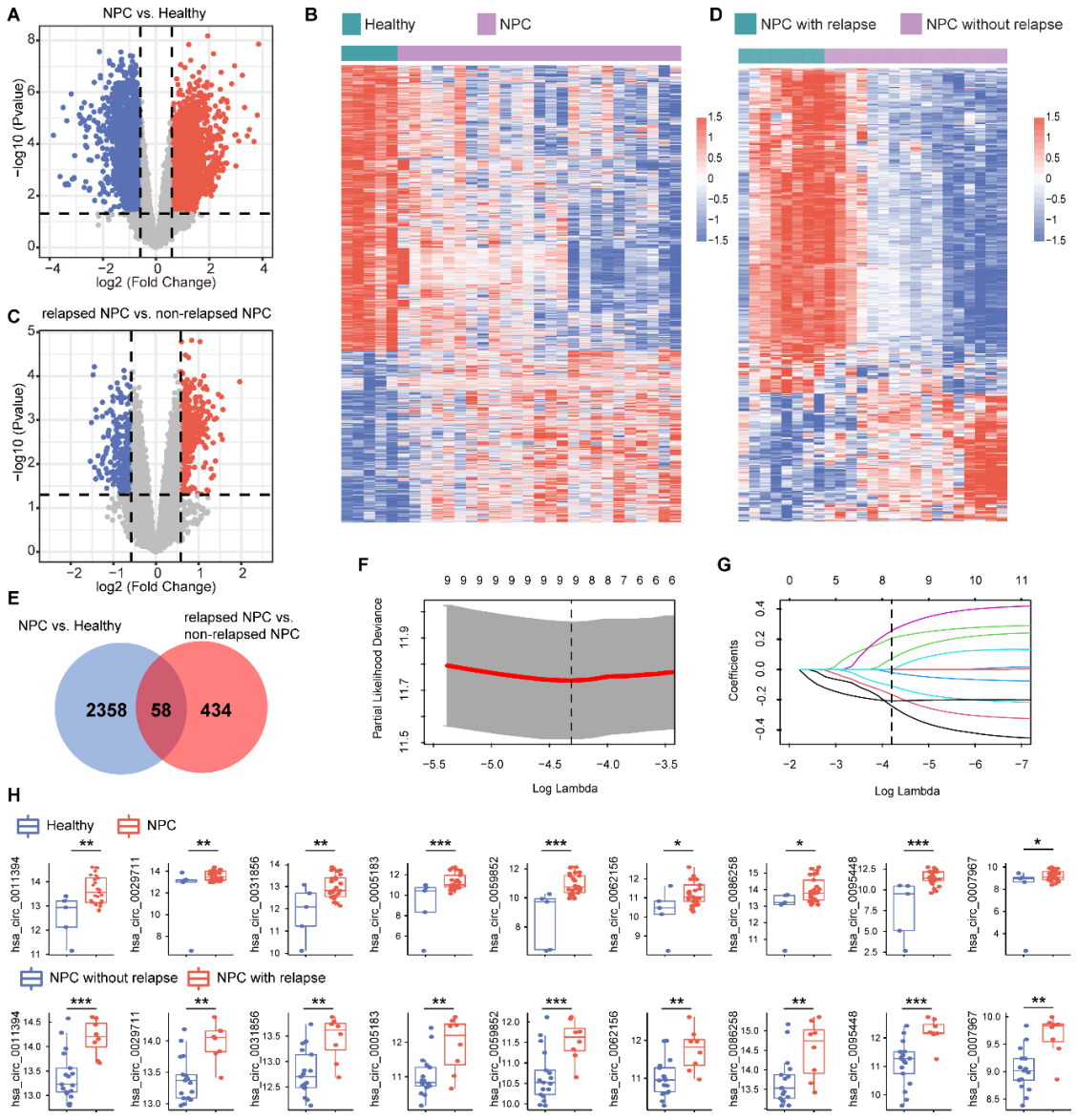

Figure S1. Relapse-related circRNAs screening with microarray, related to Figure 2.

(A)Volcano plot of circRNA profiling between LA-NPC and healthy groups. (B) Expression profiling of differentially expressed circRNAs between LA-NPC and healthy groups. (C)Volcano plot of circRNA profiling between relapsed LA-NPC and non-relapsed LA-NPC groups. (D) Expression profiling of differentially expressed circRNAs between relapsed LA-NPC and non-relapsed LA-NPC groups. (E) Venn plot showing intersection of the upregulated circRNAs. (F) Ten-time cross-validations to tune the parameter selection in the LASSO model. (G) LASSO coefficient profiles of the candidate proteins for PSDM construction. (H) Box plots showing the expression of the nine circRNA included in the classifier in LA-NPC vs. normal nasopharyngeal tissues (up), and in non-relapsed LA-NPC vs. relapsed LA-NPC. *P*-values were based on empirical Bayes statistics. *$P < 0.05$, ** $P < 0.01$, *** $P < 0.001$.

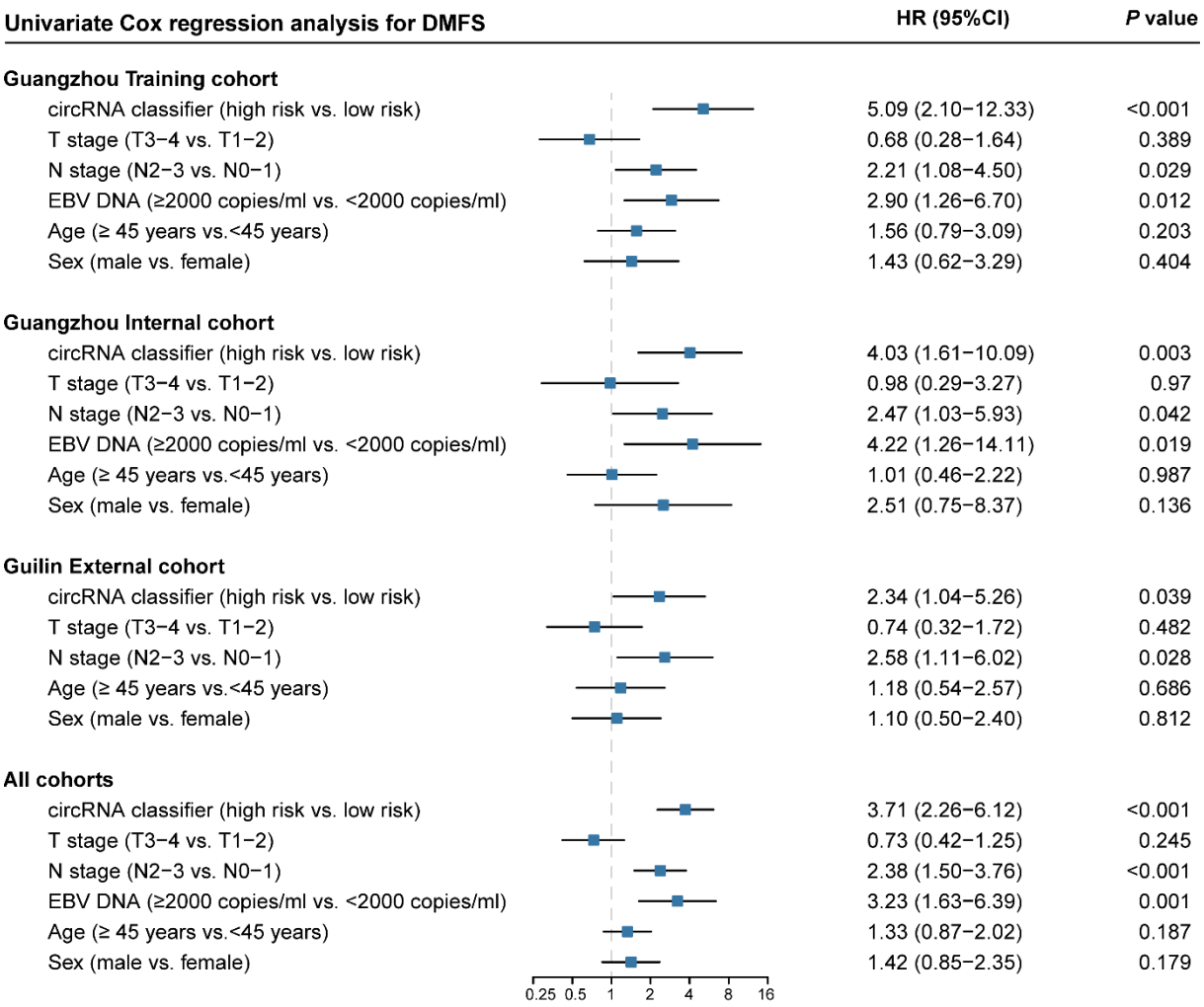

Figure S2. Univariate association of circRNA classifier and clinicopathological characteristics with distant metastasis-free survival, related to Figure 2.

P values and hazard ratios were based on univariate Cox regression analyses.

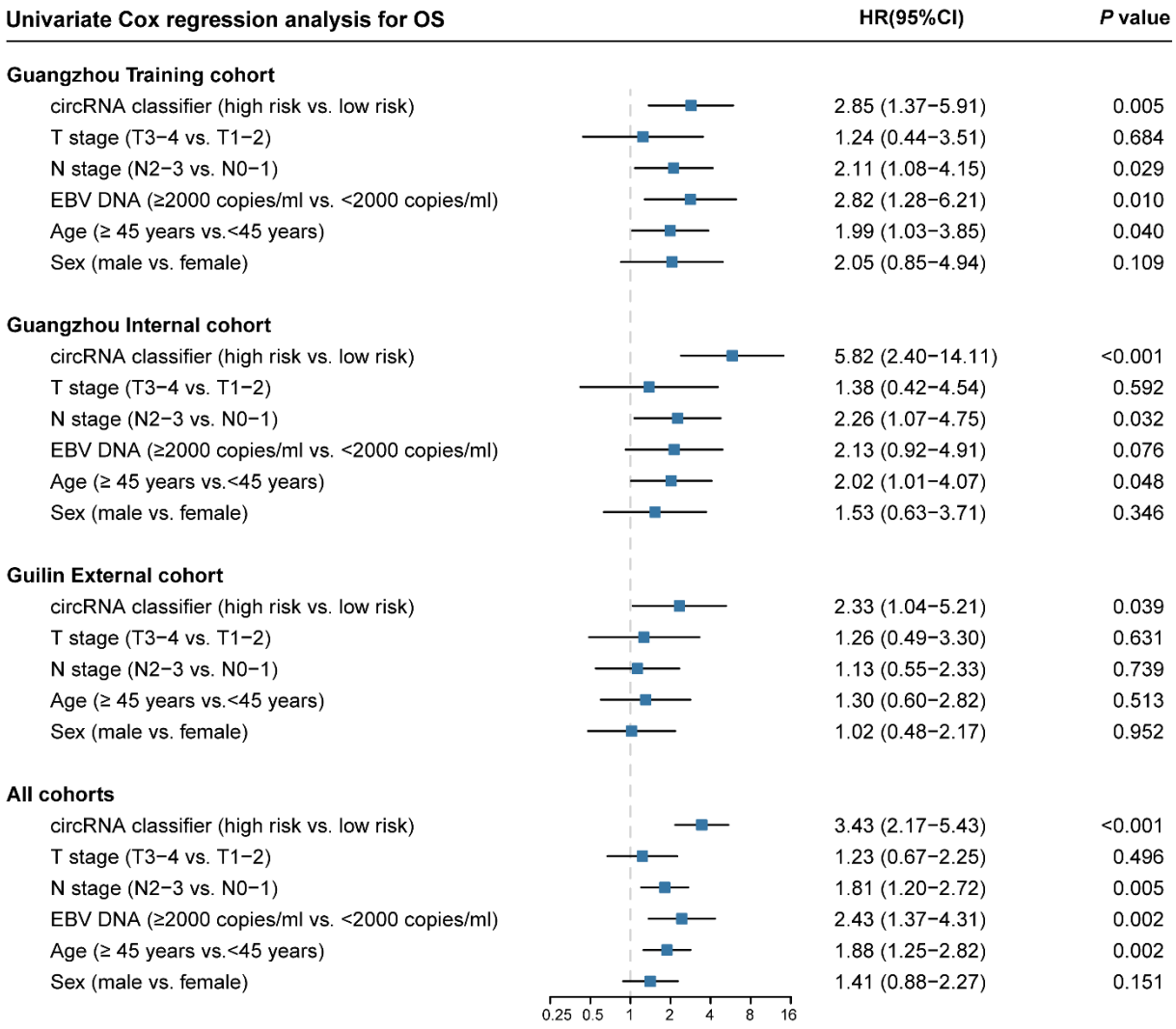

Figure S3. Univariate association of circRNA classifier and clinicopathological characteristics with overall survival, related to Figure 2.

P values and hazard ratios were based on univariate Cox regression analyses.

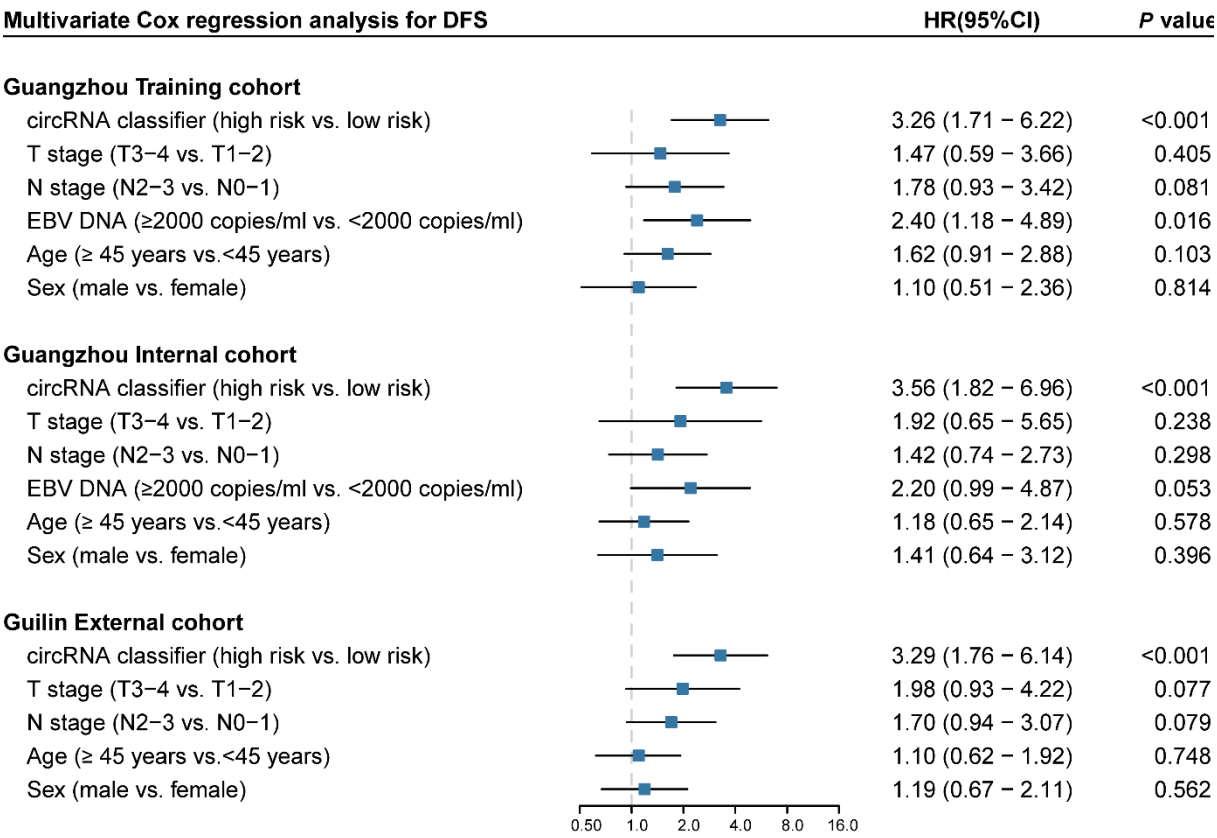

Figure S4. Multivariate association of the circRNA classifier and clinicopathological characteristics with disease-free survival, related to Figure 4.

We calculated hazard ratios and *P* values using a multivariate Cox proportional hazards regression model. EBV, Epstein-Barr virus; HR, hazard ratio; CI, confidence interval.

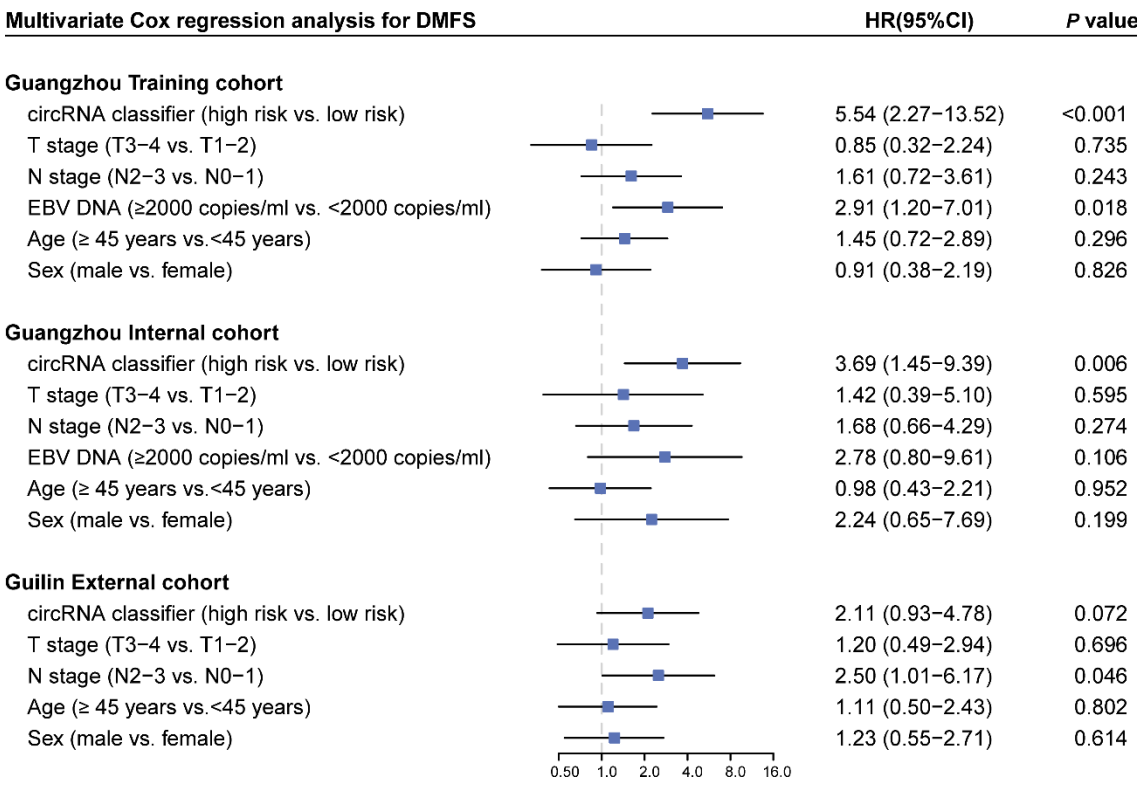

Figure S5. Multivariate associations of the circRNA-based classifier and clinicopathological characteristics with distant metastasis-free survival, related to Figure 4.

We calculated hazard ratios and *P* values using multivariate Cox proportional hazards regression model. EBV, Epstein-Barr virus; HR, hazard ratio; CI, confidence interval.

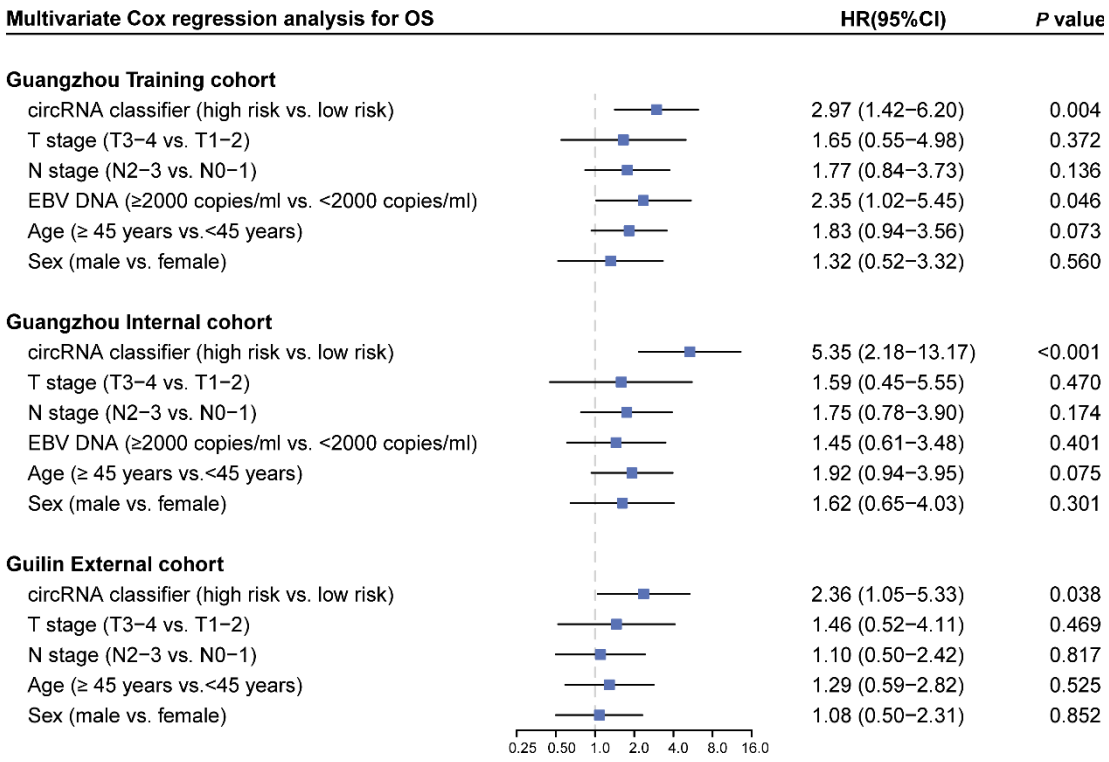

Figure S6. Multivariate associations of the circRNA classifier and clinicopathological characteristics with overall survival, related to Figure 4.

We calculated hazard ratios and *P* values using multivariate Cox proportional hazards regression model. EBV, Epstein-Barr virus; HR, hazard ratio; CI, confidence interval.

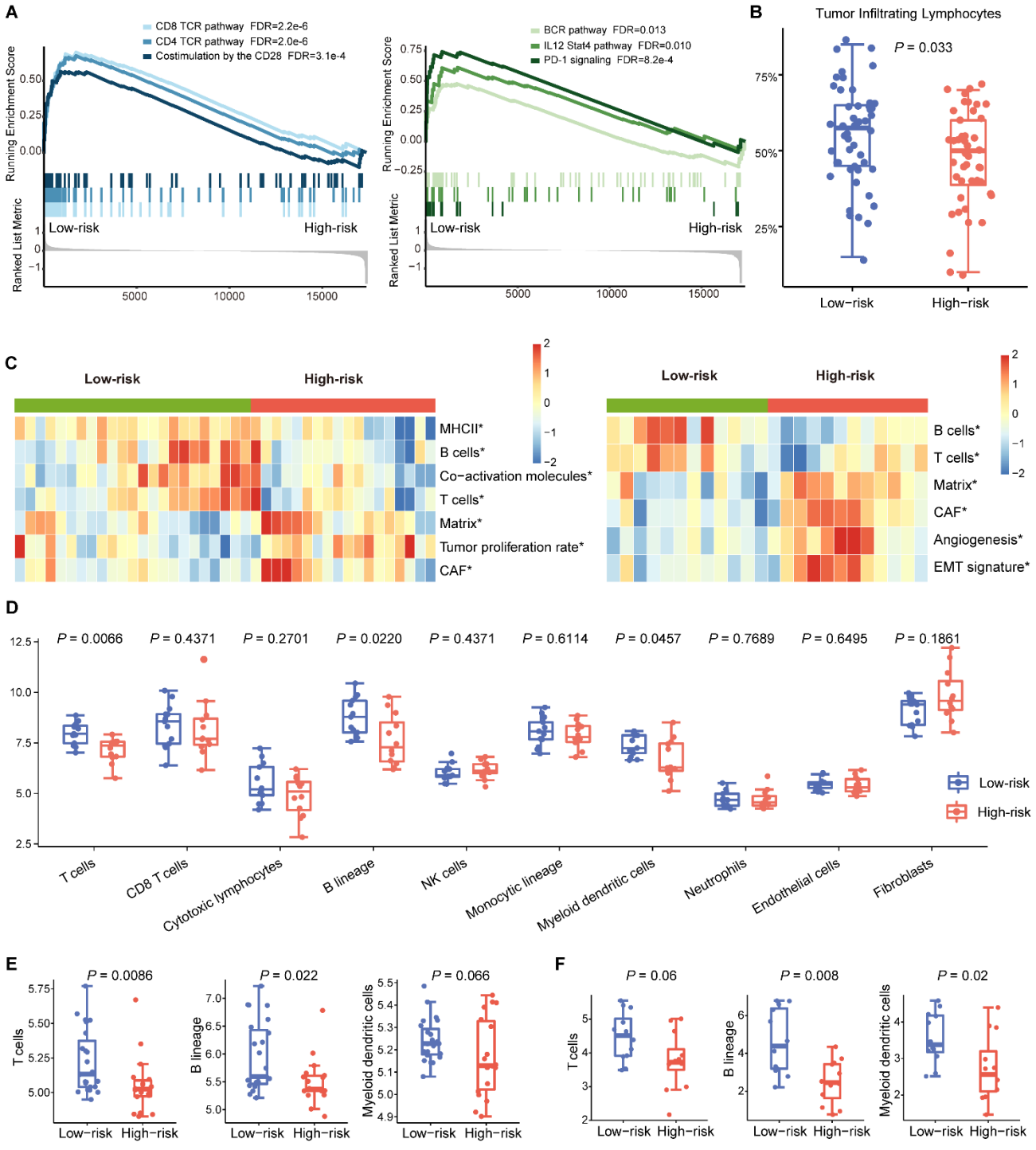

Figure S7. Immune characterization in the low- and high-risk group, related to Figure 5.

(A) Immune-related pathways enriched by GSEA in the low-risk group with Affymetrix HTA data. (B) Box plots showing tumor infiltrating lymphocytes evaluated on the H&E slides. (C) Heatmap of TME ssGSEA scores in NPC samples classified into low- and high-group based on the circRNA-based classifier. * P <0.05, P -values were based on a simple linear model and moderate t-statistic. (D) Gene signature scores derived from the MCP-counter cell deconvolution algorithm in the circRNA microarray data. P-values were based on the Wilcoxon rank sum test. (E) Gene signature scores derived from the MCP-counter cell deconvolution algorithm in Affymetrix HTA and RNA-seq datasets. P-values were based on the Wilcoxon rank sum test.

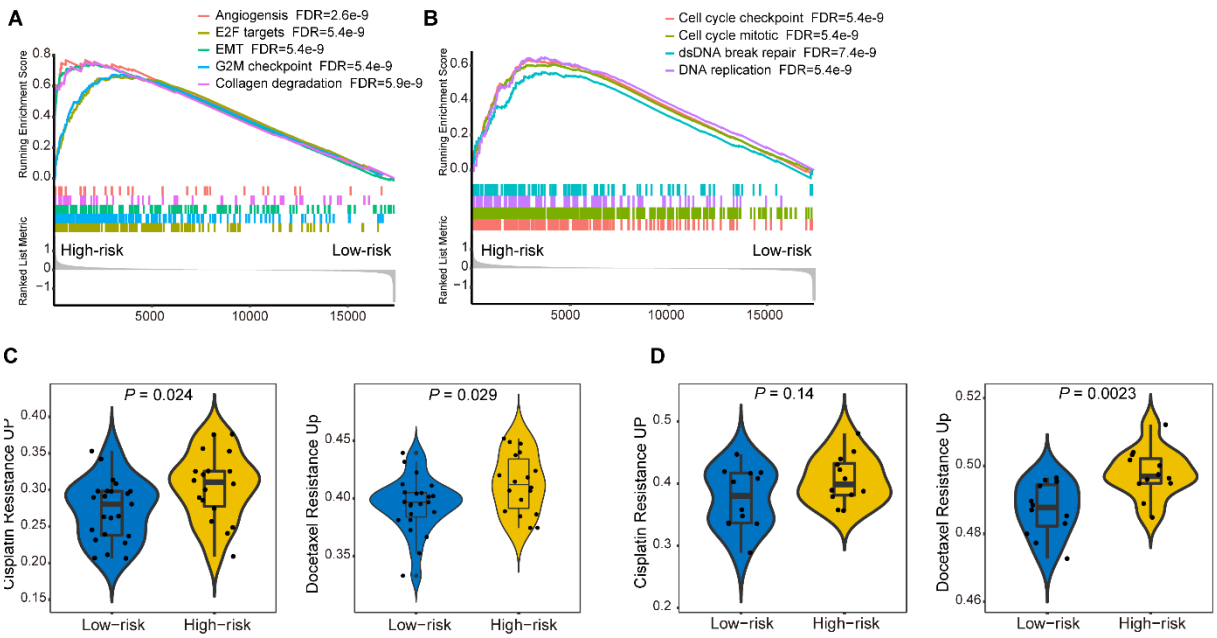

Figure S8. Pro-relapse and chemo-resistant features in the low- and high-risk group, related to Figure 6.

(A) Pro-relapse associated pathways enriched by GSEA in the high-risk group with Affymetrix HTA data. (B) Cell cycle and DNA repair associated pathways enriched by GSEA in the high-risk group with Affymetrix HTA data. (C) Violin plots showing expression of cisplatin resistance signature and docetaxel resistance signature by the Affymetrix HTA data. *P*-values were based on the Wilcoxon rank sum test. (D) Violin plots showing expression of cisplatin resistance signature and docetaxel resistance signature by the RNA-seq data. *P*-values were based on the Wilcoxon rank sum test.

Supplementary Table S1. The number of events for patients of different subtypes in all three cohorts, related to Figure 2.

	Guangzhou Training cohort (n = 170)			Guangzhou Internal cohort (n = 170)			Guilin external cohort (n = 150)		
	Subtype L (n = 85)	Subtype H (n = 85)	*P*	Subtype L (n = 90)	Subtype H (n = 80)	*P*	Subtype L (n = 66)	Subtype H (n = 84)	*P*
Number of events									
Disease progression	13	34	0.001	12	34	<0.001	13	44	<0.001
Distant metastasis	6	27	<0.001	6	19	0.002	8	22	0.040
Death	10	26	0.004	6	27	<0.001	8	23	0.026

Supplementary Table S2. The 5-year survival estimates for patients of different subtypes in all three cohorts, related to Figure 2.

	Guangzhou Training cohort (n = 170)		Guangzhou Internal cohort (n = 170)		Guilin external cohort (n = 150)	
	Subtype L (n = 85)	Subtype H (n = 85)	Subtype L (n = 90)	Subtype H (n = 80)	Subtype L (n = 66)	Subtype H (n = 84)
5-year survival						
DFS (%)	85.7	63.5	88.9	61.2	76.7	45.6
(95% CI)	(78.5 – 93.5)	(54.0 – 74.6)	(82.6 – 95.6)	(50.1 – 71.7)	(65.5 – 89.8)	(35.6 – 58.3)
DMFS (%)	93.9	70.4	93.2	81.0	87.3	72.5
(95% CI)	(88.8 – 99.2)	(61.3 – 80.9)	(88.2 – 98.6)	(72.8 – 90.1)	(79.3 – 96.0)	(63.2 – 83.2)
OS (%)	91.6	75.1	94.4	72.2	86.9	67.4
(95% CI)	(85.8 – 97.7)	(66.4 – 84.9)	(89.8 – 99.3)	(62.9 – 82.8)	(78.6 – 96.0)	(56.5 – 80.5)

Abbreviations: DFS: disease-free survival; DMFS: distant metastasis-free survival; OS: overall survival; CI: confidence interval.

Supplementary Table S3. Publicly available gene sets used in this study, related to Figure 5.

Genesets	Source
Angiogenesis Antitumor cytokines B cells Cancer-associated fibroblasts (CAF) Checkpoint molecules Co-activation molecules Effector cell traffic Effector cells EMT signature Endothelium Granulocyte traffic Immune Suppression by Myeloid Cells (MDSC) M1 signature Macrophage and DC traffic Matrix Matrix remodeling MHCI MHCII Myeloid cells traffic Neutrophil signature NK cells Protumor cytokines T cells Th1 signature Th2 signature Treg Treg and Th2 traffic Tumor-associated Macrophages (TAM) Tumor proliferation rate	Bagaev, A., Kotlov, N., Nomie, K., Svekolkin, V., Gafurov, A., Isaeva, O., Osokin, N., Kozlov, I., Frenkel, F., Gancharova, O., et al. (2021). Conserved pan-cancer microenvironment subtypes predict response to immunotherapy. Cancer Cell 39, 845-865 e847. 10.1016/j.ccell.2021.04.014
Angiogenesis E2F targets Epithelial-mesenchymal transition G2M checkpoint	MsigDb hallmark gene sets
BCR Pathway CD40 Pathway CD8 TCR Pathway IL12 Stat4 Pathway CD4 TCR Pathway TNF Pathway	MsigDb PID subset of CP
Base Excision Repair Cell Cycle Checkpoints Cell Cycle Mitotic Costimulation By The CD28 Family Death Receptor Signalling DNA Double-Strand Break Repair DNA Replication Extracellular Matrix Organization PD-1 Signaling TRIF Mediated Programmed Cell Death	MsigDb REACTOME subset of CP
Tsunoda cisplatin resistance up	MsigDb
Honma Docetaxel Resistance	MsigDb